

# PACC: Protocol-Aware Cross-Layer Compression for Compact Network Traffic Representation

Zhaochen Guo

University of Electronic Science and  
Technology of China  
Chengdu, Sichuan, China  
2023310101003@std.uestc.edu.cn

Tianyufei Zhou

University of Hong Kong  
Hong Kong, China  
tianyufei.zhou@connect.hku.hk

Honghao Wang

Renmin University of China  
Beijing, China  
2023202755@ruc.edu.cn

Ronghua Li

Hong Kong Polytechnic University  
Hong Kong, China  
cory-ronghua.li@connect.polyu.hk

Shinan Liu

University of Hong Kong  
Hong Kong, China  
shinan6@hku.hk

## Abstract

Network traffic classification is a core primitive for network security and management, yet it is increasingly challenged by pervasive encryption and evolving protocols. A central bottleneck is *representation*: hand-crafted flow statistics are efficient but often too lossy, raw-bit encodings can be accurate but are costly, and recent pre-trained embeddings provide transfer but frequently flatten the protocol stack and entangle signals across layers.

We observe that real traffic contains substantial *redundancy* both across network layers and *within* each layer; existing paradigms do not explicitly identify and remove this redundancy, leading to wasted capacity, shortcut learning, and degraded generalization. To address this, we propose PACC, a redundancy-aware, layer-aware representation framework. PACC treats the protocol stack as multi-view inputs and learns compact layer-wise projections that remain faithful to each layer while explicitly factorizing representations into *shared* (cross-layer) and *private* (layer-specific) components. We operationalize these goals with a joint objective that preserves layer-specific information via reconstruction, captures shared structure via contrastive mutual-information learning, and maximizes task-relevant information via supervised losses, yielding compact latents suitable for efficient inference.

Across datasets covering encrypted application classification, IoT device identification, and intrusion detection, PACC consistently outperforms feature-engineered and raw-bit baselines. On encrypted subsets, it achieves up to a 12.9% accuracy improvement over nPrint. PACC matches or surpasses strong foundation-model baselines. At the same time, it improves end-to-end efficiency by up to 3.16 $\times$ .

## 1 Introduction

Network traffic classification is a fundamental building block for modern network security (e.g., intrusion detection [5, 23], malware analysis [33], anomaly detection [12, 29]) and network management (e.g., application identification [1, 10, 32], QoE inference [11, 19, 21], capacity planning [17, 53]). As network protocols and applications evolve, the problem has also shifted: today, the majority of traffic payload is encrypted [3], making “what can be observed” in raw packets and flows a moving target.

Over the past decades, the community has developed a sequence of traffic representation paradigms. Early systems relied on *coarse-grained flow statistics* [10, 18, 40, 47] (e.g., packet size distributions,

inter-arrival times, burstiness, and summary counters). These features [15, 35, 39] are computationally efficient and easy to deploy, however, they discard fine-grained evidence. Moving forward, *raw-bit (or raw-byte) representations* directly encode packet headers and payload bytes for deep models (e.g., Deep Packet [20] and nPrint-style [7, 9] encodings). These representations can be accurate, but they are often sparsely high-dimensional and computationally expensive, yielding thousands of bits/tokens per flow, increasing training difficulty and inference cost. More recently, *pre-trained model embeddings* [6, 14, 52] have emerged as a compelling alternative: they amortize knowledge into a large backbone and provide a strong transfer. However, many embedding pipelines treat traffic as a monolithic sequence and thereby *ignore the hierarchical structure of the protocol stack*; they tend to entangle signals across layers and suffer performance degradation under downstream domain shifts.

Moreover, none of the aforementioned traffic representation paradigms is designed to reflect one key insight: *network traffic exhibits substantial redundancy both across layers and within layers*. In this paper, we take a systematic view of redundancy in network traffic. Raw packet streams contain substantial *layer-specific redundancy*—repetitive header fields, predictable counters, and session-specific artifacts—that inflates representations and consumes computational budget. At the same time, the protocol stack repeatedly encodes related semantics across layers; these cross-layer correlations form *cross-layer redundancy*, or consensus, that provides robust evidence for classification. Accordingly, our goal is not to frame redundancy as a single nuisance, but to *compress repetitive information, align shared evidence across layers, and retain distinctive layer-specific cues* that strengthen complementarity. Fig. 1 illustrates the shared–private principle for cross-layer traffic on two layers.

Motivated by this, we propose PACC, a cross-layer traffic representation framework that *systematically exploits redundancy* to produce compact and generalizable features. PACC treats the protocol stack as a set of *layer views* and learns (i) compact layer-wise projections that preserve essential information, (ii) an explicit separation between *shared* information (redundant across layers) and *private* information (layer-specific information), and (iii) a joint optimization strategy that encourages the final representation to be *informative for downstream tasks* while keeping redundant capacity usage in check. At a high level, PACC is guided by three

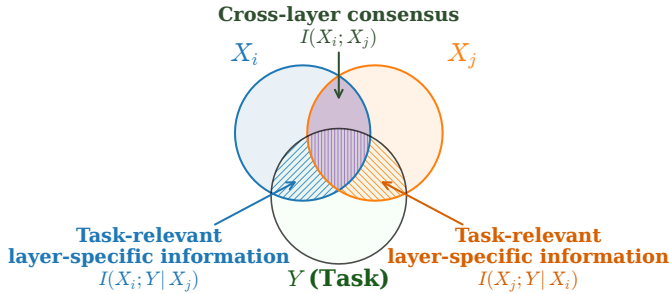


**Figure 1: Illustration of the shared-private principle for cross-layer traffic. We seek representations that capture both cross-layer consensus  $I(X_i; X_j)$  and layer-specific, task-relevant evidence such as  $I(X_i; Y | X_j)$ .**

design principles: **(P1) Layer-awareness:** respect protocol hierarchy instead of flattening it; **(P2) Redundancy control:** explicitly model shared vs. unique information to reduce duplicated signals across layers; and **(P3) Efficiency without sacrificing accuracy:** compress high-dimensional raw encodings into compact latents suitable for scalable training and low-latency inference.

We evaluate PACC on multiple traffic classification settings, including encrypted application classification, IoT device classification, and intrusion detection, and compare against feature-engineered methods, raw-bit baselines, and pre-trained embedding approaches. Overall, the results show that protocol-aware cross-layer representations can substantially improve practical accuracy/robustness relative to traditional features, while remaining efficient and competitive against large pre-training pipelines. PACC also provides interpretability at the layer level: it clarifies *which layers* are contributing shared versus unique evidence, which is valuable for debugging and for deployments under partial observability. We summarize our main contributions as follows:

- We formalize network traffic as *cross-layer "multiview" data* and motivate redundancy as a first-class property that impacts both efficiency and generalization.
- We empirically analyze redundancy in raw cross-layer traffic using information-theoretic and compression-based measures, demonstrating substantial redundancy across and within layers.
- We propose PACC, a redundancy-aware cross-layer representation framework that learns compact, task-relevant representations by modeling shared and private information across layers.
- We conduct extensive experiments across diverse datasets and objectives, showing that PACC improves over feature-engineered and raw-bit baselines and is competitive with modern pre-training approaches, while enabling efficient inference.

## 2 Background and Motivation

### 2.1 Network Traffic & Representations

A network flow is a temporally ordered sequence of packets exchanged between two endpoints. Each packet is structured by the protocol stack, meaning that a single communication event leaves traces at multiple layers. Headers at the link, network, and transport layers expose metadata and control semantics, while the application layer (often encrypted [30]) contributes higher-level behavior that

still manifests through side channels such as record sizes, burst patterns, and timing.

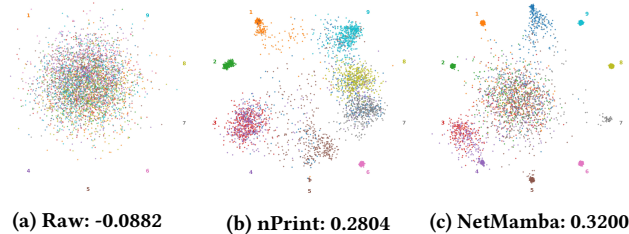
In the context of traffic analysis, a **representation** is a structured abstraction of network flows on a feature space that captures the underlying communication patterns [16, 43, 46]. While the layered organization of flow packets naturally suggests a multiview abstraction, existing traffic representations compress and organize the evidence in different ways. **Flow statistics** aggregate packets into summary counters and distributions [15, 35, 39] (counts, size histograms, inter-arrival summaries, burst metrics). They are lightweight and naturally condense large amounts of within-layer repetition, yet this aggregation also smooths out fine-grained cross-layer agreement and rare but discriminative events. As encryption and protocol evolution reduce stable plaintext cues, these coarse summaries can become fragile across environments. In recent years, the following two trends have been significantly more favored: **Raw-bit/byte encodings** preserve packet structure more directly by encoding headers [22, 37, 42, 45, 50] (and sometimes payload bytes [8]) as high-dimensional sequences. They can be accurate, but the sequences contain substantial syntactic repetition (predictable header fields) and session-specific artifacts alongside genuinely useful evidence, which increases both compute cost and the risk of learning incidental correlations. **Pre-trained embeddings** demonstrate superior performance on downstream tasks [14, 27, 51, 52]. However, many pipelines flatten the raw-bit protocol stacks into a single stream. This makes it harder to reason about which evidence recurs across layers as shared consensus versus which evidence is distinctive to a given layer and therefore complementary.

Fig. 2 illustrates the class-level distinguishability of the current representation learning paradigms in a two-dimensional feature space, where the coordinates are projected based on the pseudo-probability vectors and prediction confidence values derived from category-wise probability distributions. The negative Silhouette coefficient [31] of *Raw-bit representations* (-0.0882) demonstrates that the raw feature space exhibits high degrees of chaos, rendering it inherently challenging to directly retrieve task-relevant information amid excessive syntactic redundancy. Although *Monolithic embeddings* (e.g., nPrint [7] and NetMamba [41]) project flattened raw-bit stacks into a latent space to enhance representational quality—achieving higher Silhouette coefficients (0.2804 and 0.3200, respectively)—their clustering results still suffer from substantial category ambiguity and spurious noise.

Driven by the entanglement of decision boundaries observed in the aforementioned representations, this work puts forward two core insights:

- The chaotic nature of raw-bit features may introduce excessive redundant information into direct representation learning processes, hindering the extraction of task-relevant features.
- Even when compressing across layer-stacks, such operations may amplify the contributions of non-significant feature components while attenuating the importance of principal components that dominate task performance.

Accordingly, this work aims to explore a more robust representation paradigm, namely *cross-layer multiview abstraction*. This paradigm treats individual layers (or layer groups) as distinct views prior to



**Figure 2: Representation structure on CipherSpectrum-4. Two-dimensional projections of node representations with Silhouette scores.**

fusion, with its learning objective adhering to a dialectical perspective on redundancy: it consolidates layer-specific repetitions into compact latent representations while aligning shared discriminative evidence across layers, without compromising distinctive cues that enhance cross-layer complementarity.

**Representation optimization in other domains.** Prior work on multiview or multimodal representation learning often decomposes an input into aligned modalities and reports two recurring gains. First, *contrastive alignment* uses cross-modal agreement as supervision [24, 28, 36, 48]; by rewarding information that is shared across modalities, these objectives tend to highlight stable semantic evidence while reducing dependence on modality-specific syntactic repetition and environment-dependent noise that do not align across views. Second, *multimodal fusion* methods integrate modality-specific features into a joint embedding that preserves complementary signals and often improves over uni-modal baselines [4, 38, 49]. These results suggest an analogous design for encrypted-traffic representation learning: treating protocol layers as separate but correlated modalities and learning both cross-layer consensus and layer-specific information can help mitigate the brittleness of features derived from any single layer.

## 2.2 Redundancy Analysis

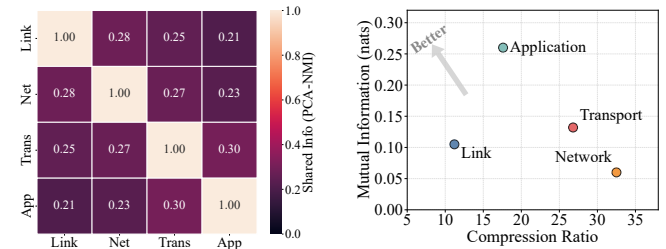
Redundancy in multi-layer network traffic traces has two roles:

**Cross-layer redundancy/consensus.** Different layers encode coupled aspects of the same communication event, so related semantics are echoed throughout the stack. Even with strong encryption, application behavior induces consistent patterns that propagate into transport and network metadata (e.g., handshake dynamics, burst structure, length-related fields). This cross-layer agreement is often robust evidence for classification.

**Layer-specific redundancy/information.** Many header fields are constant within a protocol version, predictable from neighboring fields, or only weakly coupled to the downstream label (e.g., checksums, ephemeral identifiers, session-specific counters). These bits inflate raw representations and occupy compute without necessarily improving task performance.

We quantify these phenomena by examining cross-layer dependence ( $I(X_i; X_j \mid Y)$ ) to assess view agreement, alongside layer-specific task relevance ( $I(X_i; Y)$ ) and redundancy (proxied by compression ratios) in Fig. 3.

The results reflect the dialectical structure of redundancy. In Fig. 3a, raw encodings exhibit moderate shared information across most layer pairs ( $\approx 0.21\text{--}0.30$  off-diagonal), capturing a blend of



**(a) Cross-layer consensus**      **(b) Layer-specific information**

**Figure 3: Layer-wise perspective on NMI and compression.** (a) Task-relevant Cross-layer PCA-normalized conditional mutual information  $I(X_i; X_j \mid Y)$ . (b) Task relevance quantified by  $I(X_i; Y)$  (higher is better) and redundancy proxied by the compression ratio (lower implies compactness).

representational coupling, while implicitly signifying the existence of layer-specific information that remains uncoupled.

The quantitative analysis in Fig. 3b reveals a striking structural mismatch across layers, most notably within the network layer. Not only maximizing redundancy (compressing by  $> 30\times$ ), it also offers minimal *task relevance* ( $I(X_i; Y) < 0.10$  nats). This "high-redundancy, low-relevance" profile encapsulates the fundamental challenge of raw-traffic learning: the discriminative "signals" are needles in a haystack of protocol-mandated "noise".

Ideally, traffic abstraction requires **discriminative distillation**: filtering task-irrelevant protocol overhead via compression, while simultaneously amplifying cross-layer redundancy to harvest consensus signals.

## 3 Problem Formulation

We study network traffic analysis under a *cross-layer, multiview* abstraction. Given a dataset of  $N$  flows with labels  $Y \in \{1, \dots, C\}$ , we represent each flow using  $M$  views (network layers)  $X = \{X_1, \dots, X_M\}$ , where each view  $X_i \in \mathbb{R}^{N \times d_f}$  corresponds to a specific network layer (e.g., L2/L3/L4 headers and L7 payload content<sup>1</sup>). Our goal is to learn a *compact* representation that is accurate, efficient, and robust even under encryption.

Formally, we aim to learn (i) layer-specific encoders  $f_{\Theta_i}$  that map each layer to a low-dimensional latent  $Z_i = f_{\Theta_i}(X_i)$ , and (ii) a fusion/classifier head  $h_{\Phi}$  that predicts  $\hat{Y} = h_{\Phi}(Z_1, \dots, Z_M)$ . A key challenge is that raw traffic's stacked protocol structure is inherently redundant. Naive concatenation creates an exploded feature space, exacerbating the *curse of dimensionality*; conversely, collapsing all layers into a single embedding can entangle signals and obscure which information is shared versus complementary.

This motivates the following desiderata for cross-layer traffic representations:

- (1) **Layer fidelity.** Each  $Z_i$  should preserve essential information from its corresponding raw feature  $X_i$  while reducing dimensional redundancy (i.e., avoid collapsing away useful layer-specific cues).

<sup>1</sup>Although all protocol layers collectively form a unified information source, commercial packet capture tools primarily provide access to L2–L4. In encrypted settings, L7 content is generally unavailable and might be omitted.

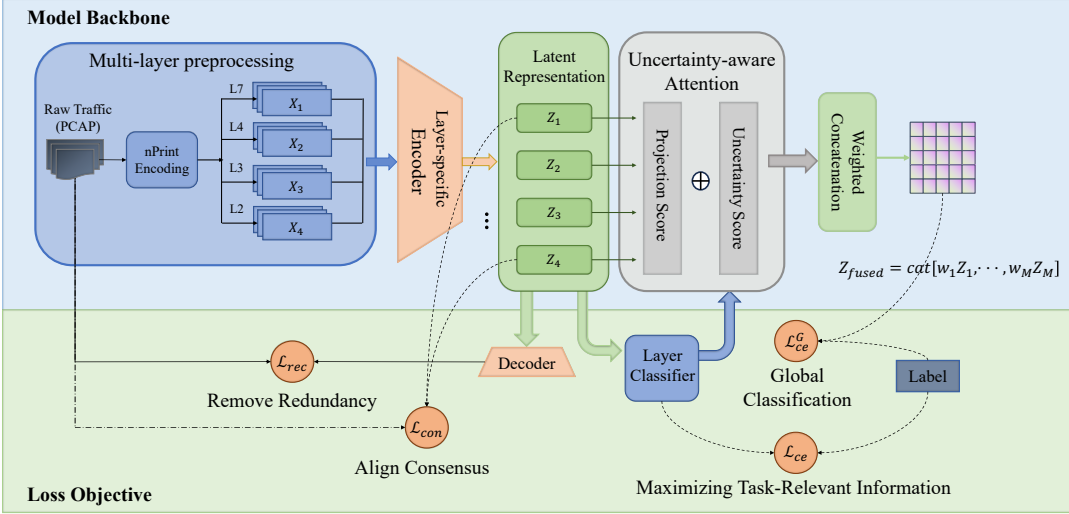


**Figure 4: The overall framework of PACC.** It consists of two main parts: the **Model Backbone** and the **Loss Objective**. The backbone extracts multi-layer representations ( $Z_1$  to  $Z_4$ ) from raw traffic using nPrint encoding and fuses them via an **Uncertainty-aware Attention** mechanism. The model is optimized jointly using reconstruction loss ( $\mathcal{L}_{rec}$ ), consensus loss ( $\mathcal{L}_{con}$ ), and classification losses ( $\mathcal{L}_{ce}$ ,  $\mathcal{L}_{ce}^G$ ).

- (2) **Redundancy-aware complementarity.** The final representation should capture task-relevant information from two essential dimensions. First, it should leverage *shared information* across layers as valuable signal reinforcement, emphasizing inter-layer consistency to improve robustness. Second, it must explicitly capture *layer-specific* information that provides unique, complementary evidence. Thus, as shown in figure 1, we aim to integrate shared consensus, represented by  $I(X_i; X_j)$ , while identifying non-redundant task-relevant contributions captured by  $I(X_i; Y | X_j)$  in Definition 3.1.
- (3) **Compactness and efficiency.** The representation should be substantially smaller than raw-bit encodings to enable scalable training and low-latency inference.

**Multiview data non-redundancy.** Task-relevant information exists not only in the shared information between views but also potentially within the unique information of certain view. Following the non-redundancy principle [13], we provide the formal definition of Multiview data non-redundancy.

**DEFINITION 3.1.**  $X_i$  is considered non-redundant with  $X_j$  for  $Y$  if and only if there exists  $\epsilon > 0$  such that the conditional mutual information satisfies  $I(X_i; Y | X_j) > \epsilon$  or  $I(X_j; Y | X_i) > \epsilon$ .

Therefore, the problem we address is: *how can we learn a cross-layer representation that (i) remains faithful to each layer, (ii) explicitly separates shared versus layer-specific information to control redundancy, and (iii) improves generalization and efficiency for downstream traffic classification?* In the next section, we present PACC, which operationalizes these goals by learning compact layer-wise projections and modeling shared information across layers.

## 4 Methodology

As illustrated in Fig. 4, this section details how PACC enhances cross-layer consensus and layer-specific signals while reducing redundancy for downstream tasks. The framework employs a shared backbone to fuse multi-layer representations via uncertainty-aware attention, trained with a joint objective combining reconstruction, consensus, and classification losses.

### 4.1 Multi-layer Projection

Raw packet embeddings (e.g., nprint) often contain excessively redundant 0/1 padding for absent control fields, impeding the efficient construction of layer-specific representations. To address this, PACC projects high-dimensional features into representations  $Z_i$  that capture essential information from raw features  $X_i$  while reducing dimensionality. We maximize the mutual information  $I(X_i; Z_i)$  to encourage projections to retain maximal intrinsic layer information. Formally, this objective is defined as:

$$\arg \max_{\Theta_i} I(X_i; Z_i), \quad Z_i = f_{\Theta_i}(X_i), \quad (1)$$

where  $f_{\Theta_i}$  denotes the layer-specific encoder parameterized by  $\Theta_i$ . This maximization ensures  $Z_i$  preserves essential layer-specific details, yielding compact representations optimized for downstream cross-layer integration.

As directly estimating  $I(X_i; Z_i)$  is intractable, we maximize a lower bound by minimizing the conditional entropy  $H(X_i | Z_i)$ , effectively reducing uncertainty in feature recovery. In practice, we use a similarity-based reconstruction loss to prioritize *directional alignment*. This suits binary nPrint embeddings, where representative identity resides in the *spatial pattern* (vector orientation) rather than magnitude. Specifically, using a parameterized decoder  $\hat{X}_i = g_{\phi}(Z_i)$ , we formulate the loss as the expected cosine distance:

$$\mathcal{L}_{\text{rec}}^i = \frac{1}{N} \sum_{k=1}^N \left( 1 - \frac{X_i^{k\top} \hat{X}_i^k}{\|X_i^k\| \|\hat{X}_i^k\|} \right). \quad (2)$$

We establish the theoretical grounding of this geometric objective as follows:

**Proposition 4.1.** *Minimizing the reconstruction loss  $\mathcal{L}_{\text{rec}}^i$  is equivalent to maximizing the variational lower bound of the mutual information  $I(X_i; Z_i)$ , thereby encouraging the latent representation  $Z_i$  to retain faithful, layer-specific information.*

The proof can be found in Appendix A.1.

## 4.2 Maximizing Cross-layer Shared Information

Having filtered *intra-layer redundancy* via projection, we focus on exploiting intrinsic *cross-layer redundancy* ( $I(X_i; X_j)$ ). We interpret this correlation as a *shared consensus* derived from unified communication intent, serving as a robust anchor against layer-specific noise. To operationalize this, we model the latent space to reflect this compositional structure, positing that  $Z_i$  contains a distinct component,  $Z_i^s$ , for this shared information.

**DEFINITION 4.1.** *Conditional Latent Decomposition Assumption.* Each layer representation  $Z_i$  consists of a shared component  $Z_i^s$  and a private component  $Z_i^u$ , denoted as  $Z_i = (Z_i^s, Z_i^u)$ . Here,  $Z_i^s$  represents the information common across layers, while  $Z_i^u$  denotes layer-specific unique information. We assume that the shared component captures all information relevant for cross-layer alignment, while the private component encodes residual information. Formally, the private component is conditionally independent of other layer representations given the shared component:  $Z_i^u \perp Z_j \mid Z_i^s, \forall j \neq i$ .

**Theorem 4.1.** *Equivalence of Shared and Holistic Mutual Information.* Maximizing the MI between the holistic representations  $Z_i$  and  $Z_j$  is equivalent to maximizing the MI between their shared components  $Z_i^s$  and  $Z_j^s$ . Under the independence assumptions in Definition 4.1, the identity  $I(Z_i; Z_j) = I(Z_i^s; Z_j^s)$  holds.

It provides an idealized justification for aligning representations via shared components. The proof can be found in Appendix A.2.

**Optimization Objective.** Theorem 4.1 suggests that capturing shared consensus  $Z^s$  does not require complex architectural disentanglement; maximizing the mutual information between embeddings  $Z_i$  and  $Z_j$  is sufficient. Since directly computing  $I(Z_i; Z_j)$  is intractable in high-dimensional spaces, we employ Contrastive Learning to maximize the differentiable InfoNCE lower bound [26].

For any layer pair  $i$  and  $j$ , the lower bound  $I_{\text{lb}}$  is defined as:

$$I_{\text{lb}}(Z_i; Z_j) = \mathbb{E}_{z_i, z_j^+ \sim p(z_i, z_j)} \left[ \log \frac{\exp f(z_i, z_j^+)}{\sum_{k=1}^N \exp f(z_i, z_j^{(k)})} \right], \quad (3)$$

where  $f(\cdot, \cdot)$  is a scoring function (implemented as a non-linear projection followed by cosine similarity). Here,  $(z_i, z_j^+)$  forms a positive pair (multi-layer views of the same sample), while  $\{z_j^{(k)}\}_{k=1}^B$  comprises one positive and  $B - 1$  negative samples.

To enforce shared consensus across the protocol stack, we aggregate this objective over all layer pairs. The final contrastive

consensus loss is formulated as:

$$\mathcal{L}_{\text{con}} = -\frac{2}{M(M-1)} \sum_{i=1}^M \sum_{j=i+1}^M I_{\text{lb}}(Z_i; Z_j). \quad (4)$$

Minimizing  $\mathcal{L}_{\text{con}}$  aligns representations of the same communication event across layers, ensuring the encoder extracts the common information essential for robust classification.

## 4.3 Maximizing Shared and Unique Information w.r.t. Downstream Task

While consensus alignment is crucial, relying on it alone is insufficient. First, straightforward alignment may preserve *task-irrelevant noise*—consistent cross-layer patterns that contribute little to classification. Second, it risks discarding *non-redundant* information unique to specific protocols (e.g., L7 payload signatures vs. L4 flow statistics) that provides complementary evidence. To address this, we maximize the mutual information between the representation and the label,  $I(Z_i; Y)$ . This acts as a dual-purpose filter: purging shared noise while extracting the unique value of each layer, ensuring all retained information is discriminative.

**4.3.1 Holistic Task-Relevant Information Pursuit.** Ideally, one might maximize only the unique task-relevant information,  $I(Z_i; Y \mid Z_{-i})$ . However, filtering shared signals is suboptimal, as it discards consensus essential for robust prediction and increases optimization complexity. Instead, we maximize the *total* task-relevant information  $I(Z_i; Y)$ , encompassing both contributions.

We establish that optimizing this holistic objective is tractable and implicitly enforces a dual decomposition of information utility, as formalized below:

**Proposition 4.2.** *Optimization and Decomposition of Task-Relevant Information.* Maximizing the total task-relevant information  $I(Z_i; Y)$  is mathematically equivalent to minimizing the standard cross-entropy loss  $\mathcal{L}_{\text{ce}}$  via a variational lower bound. Furthermore, this optimization implicitly maximizes two complementary information components:

(1) *Inter-Layer decomposition: The sum of layer-specific evidence and cross-layer consensus:*

$$I(Z_i; Y) = I(Z_i; Y \mid Z_{-i}) + I(Z_i; Z_{-i}; Y). \quad (5)$$

(2) *Intra-Layer decomposition: The sum of private feature utility and shared feature utility conditioned on private features:*

$$I(Z_i; Y) = I(Z_i^u; Y) + I(Z_i^s; Y \mid Z_i^u). \quad (6)$$

The proof can be found in Appendix A.3.

**4.3.2 Dual Implications of Information Decomposition.** Proposition 4.2 highlights the framework’s dual advantages, bridging inter-layer dynamics with intra-layer efficiency. From an inter-layer perspective, Eq. (5) shows that maximizing  $I(Z_i; Y)$  implicitly captures both layer-specific evidence  $I(Z_i; Y \mid Z_{-i})$  and task-relevant consensus  $I(Z_i; Z_{-i}; Y)$ . The former preserves unique contributions, while the latter retains shared information essential for prediction. From an intra-layer perspective, Eq. (6) reveals that maximizing  $I(Z_i; Y)$  simultaneously forces the private component  $Z_i^u$  to be predictive and reinforces the task-relevance of the shared component  $Z_i^s$ . This ensures no useful signal—whether globally shared or locally private—is discarded.

**4.3.3 Implementation via Variational Lower Bound.** As shown in Proposition 4.2, minimizing standard cross-entropy loss maximizes the mutual information lower bound. Accordingly, we define the optimization objective as:

$$\mathcal{L}_{\text{ce}} = -\frac{1}{M} \sum_{i=1}^M \sum_{c=1}^C y_{ic} \log(\hat{y}_{ic}), \quad (7)$$

where  $M$  is the number of layers,  $C$  the class count,  $y_{ic}$  the ground truth, and  $\hat{y}_{ic} = q_{\theta}(c | z_i)$  the predicted probability. This objective drives each layer to extract maximally task-relevant features.

#### 4.4 Uncertainty-Aware Fusion and Joint Optimization

The discriminative power of protocol layers is inherently non-uniform across traffic classes. Static fusion strategies fail to adapt to this *representational heterogeneity*, treating layers equally and often leading to feature dilution. To address this, we introduce an Uncertainty-Aware Supervised Attention mechanism. This module dynamically re-weights each layer by evaluating its representation quality, thereby mitigating feature dilution.

**4.4.1 Dynamic Importance Estimation.** Our fusion strategy assigns an importance weight  $w_i$  to each layer based on two properties:

(1) **Intrinsic Feature Salience (Projection Score):** We estimate structural significance using a gating network  $h(\cdot)$  (MLP with Tanh activation) mapping the embedding to a scalar score  $[-1, 1]$ :

$$s_i^{\text{proj}} = h(\tanh(W_f Z_i)), \quad (8)$$

where  $W_f$  is a learnable projection matrix.

(2) **Predictive Reliability (Uncertainty Score):** A representation is valuable only if it yields decisive classification. We quantify this via the entropy  $H(Y | Z_i)$  of the prediction distribution. Thus, the uncertainty score is defined as:

$$s_i^{\text{unc}} = -H(Y | Z_i) = \sum_{c=1}^C p(y_{ic} | Z_i) \log p(y_{ic} | Z_i). \quad (9)$$

The final attention score is  $S_i = \lambda_1 s_i^{\text{proj}} + \lambda_2 s_i^{\text{unc}}$ , where  $\lambda_1, \lambda_2$  are balancing coefficients. The normalized weights  $w_i \in \mathbb{R}^M$  are obtained via a temperature-scaled Softmax:

$$w_i = \frac{\exp(S_i/\tau)}{\sum_{j=1}^M \exp(S_j/\tau)}, \quad (10)$$

where  $\tau$  controls distribution sharpness. The fused representation is constructed by concatenating the weighted embeddings:  $Z_{\text{fused}} = [w_1 Z, \dots, w_M Z]$ . This ensures the decision relies on protocol layers with the strongest representational clarity for the specific sample.

**4.4.2 Overall Training Objective.** Effective uncertainty-aware fusion relies on calibrated layer representations. For  $s_i^{\text{unc}}$  to reflect quality rather than noise, each layer classifier requires explicit supervision.

We construct a holistic objective integrating intrinsic compression ( $\mathcal{L}_{\text{rec}}^i$ ), shared consensus ( $\mathcal{L}_{\text{con}}$ ), and discriminative power ( $\mathcal{L}_{\text{ce}}$

and global  $\mathcal{L}_{\text{ce}}^G$ ):

$$\mathcal{L}_{\text{total}} = \frac{1}{M} \sum_{i=1}^M \mathcal{L}_{\text{rec}}^i + \mathcal{L}_{\text{con}} + \mathcal{L}_{\text{ce}} + \mathcal{L}_{\text{ce}}^G \quad (11)$$

Here,  $\mathcal{L}_{\text{ce}}^G$  is the global cross-entropy loss on the fused representation  $Z_{\text{fused}}$ . To mitigate class imbalance [2], we apply class re-weighting  $\lambda_c = \frac{1-\beta}{1-\beta^{n_c}}$  ( $n_c$  is the sample count). As  $\beta \rightarrow 1$ , this converges to inverse class frequency weights, intensifying supervision on minority classes. Joint optimization creates a feedback loop: layer-wise supervision calibrates uncertainty estimates, while the fusion module provides a robust ensemble for final classification.

## 5 Experiments

### 5.1 Experimental Setups

**Datasets.** To verify the effectiveness of our proposed model, we conduct experiments on six open-access datasets derived from actual traffic scenarios, addressing three primary classification objectives. *Encrypted Application Classification*. This task aims to classify application traffic under encryption protocols. We concentrate on the recently proposed high-strength encrypted network traffic data, CipherSpectrum [44].<sup>2</sup> *IoT Device Classification*. To address the task of distinguishing traffic from various IoT devices, we utilized the UNSW 2018 dataset [34]. Specifically, we extracted traffic traces from the first four days, covering 16 distinct classes. *Attack Traffic Classification*. Aiming to detect malicious traffic, this study employs the CICIoT 2023 dataset [25] for binary classification, distinguishing between benign and attack instances. **Baselines** include traditional flow statistics, raw packet embeddings, and pre-training paradigms. **Implementation Details** comprise data preparation, feature engineering, model architecture and training configuration. The introduction of baselines, implementation details and **Metrics** can be found in Appendix B.

### 5.2 End-to-end Results

Table 1 presents a comprehensive performance comparison across six benchmark subsets, evaluating PACC against six representative baselines. The results demonstrate the consistent superiority of our proposed framework, particularly in challenging encrypted traffic scenarios where strict artifact masking is applied.

**5.2.1 Results Analysis.** Performance gains on the *CipherSpectrum* subsets highlight how strict masking protocols expose specific limitations across existing baselines. While both flow statistics methods suffer from an information bottleneck that smooths out fine-grained cross-layer agreement and rare but discriminative events, *FlowPrint* further loses effectiveness as the statistical shortcuts it relies on are eliminated. Conversely, whether relying on redundant bit representations or sparse graph structures, raw-bit/byte encoding approaches like *nPrint* and *TFE-GNN* are hampered by syntactic redundancy and session artifacts, which inflate computational overhead and risk learning incidental correlations. Crucially, even sophisticated pre-trained models like *NetMamba* and *YaTC* experience performance degradation. Their efficacy is constrained not

<sup>2</sup>Our experiments utilize 4 disjoint subsets generated by extracting samples from each category from the full 41-class, mirroring the data partition method described in [44]

**Table 1: Classification Results Across Various Domain Traffic Datasets.**

Dataset	Metric	Flow Statistics		Raw Packets		Pretrained Embedding		PACC
		AppScanner	FlowPrint	TFE-GNN	nPrint	YaTC	NetMamba	
<b>Task: Encrypted Application Classification</b>								
CipherSpectrum-1	ACC	0.1126	0.1238	0.5705	0.6455	0.6113	0.4659	<b>0.7155</b>
	PRE	0.1145	0.1250	0.7043	0.6290	<u>0.7066</u>	0.4932	<b>0.7211</b>
	REC	0.1126	0.1238	0.5705	0.6298	<u>0.6114</u>	0.4659	<b>0.7067</b>
	F1	0.1135	0.1244	0.5830	0.5926	0.6193	0.4748	<b>0.6934</b>
CipherSpectrum-2	ACC	0.1023	0.1148	0.4475	0.5590	<u>0.5750</u>	0.4975	<b>0.6602</b>
	PRE	0.1103	0.1271	0.4524	0.5533	<u>0.6076</u>	0.5278	<b>0.6400</b>
	REC	0.1023	0.1148	0.4475	0.5348	<u>0.5589</u>	0.4975	<b>0.5973</b>
	F1	0.1061	0.1206	0.4366	0.4984	<b>0.5823</b>	0.4937	<u>0.5625</u>
CipherSpectrum-3	ACC	0.1422	0.1544	0.6830	0.7653	0.7550	0.6025	<b>0.8575</b>
	PRE	0.1365	0.1479	0.6915	<u>0.7830</u>	0.7749	0.6097	<b>0.8673</b>
	REC	0.1422	0.1544	0.6830	0.7682	0.7550	0.6025	<b>0.8575</b>
	F1	0.1393	0.1511	0.6872	<u>0.7656</u>	0.7569	0.6013	<b>0.8577</b>
CipherSpectrum-4	ACC	0.1132	0.1248	0.7019	0.6488	0.7175	<u>0.7351</u>	<b>0.7829</b>
	PRE	0.1325	0.1446	0.7152	0.5138	0.7309	<u>0.7604</u>	<b>0.7657</b>
	REC	0.1132	0.1248	0.7019	0.6399	0.7175	<u>0.7351</u>	<b>0.7761</b>
	F1	0.1221	0.1340	0.7084	0.5492	<b>0.7177</b>	0.6964	<u>0.7099</u>
<b>Task: IoT Device Classification</b>								
UNSW 2018	ACC	0.4726	0.5179	0.9612	0.9785	0.9827	0.9849	<b>0.9938</b>
	PRE	0.2359	0.2682	0.6210	0.7701	<u>0.9835</u>	0.9828	<b>0.9875</b>
	REC	0.4721	0.5176	0.6548	0.7390	0.9741	<b>0.9849</b>	0.9795
	F1	0.3147	0.3534	0.6321	0.7516	0.9783	<u>0.9827</u>	<b>0.9831</b>
<b>Task: Attack Traffic Identification</b>								
CICIoT 2023	ACC	0.9059	0.9715	0.9558	0.9475	<u>0.9819</u>	0.9770	<b>0.9869</b>
	PRE	<u>0.9914</u>	0.9666	0.9629	0.9005	<u>0.9774</u>	0.9769	<b>0.9921</b>
	REC	<u>0.9059</u>	<u>0.9763</u>	0.9303	0.9285	0.9569	<b>0.9770</b>	0.9633
	F1	0.9451	0.9706	0.9464	0.9137	0.9682	<u>0.9769</u>	<b>0.9770</b>

only by the domain shift between upstream pre-training distributions and the randomized target domain but also by their structural reliance on specific artifacts (e.g., ports) that lose discriminative value under masking. Furthermore, treating diverse protocols as a flat sequence inevitably assimilates *task-irrelevant noise*. In contrast, PACC consistently outperforms these heavy models without relying on expensive pre-training. By explicitly modeling cross-layer *shared consensus*, it functions as a semantic filter that purges noise to capture intrinsic evidence, ensuring robustness even when transient artifacts are randomized.

**5.2.2 Redundancy Analysis.** Complementing to Fig. 3, we visualize the layer-wise perspective on mutual information and compression of PACC embeddings in Fig. 5. As shown in Fig. 5a, PACC reshapes the consensus pattern: shared evidence becomes more concentrated among Network/Transport/Application (up to  $\approx 0.35\text{--}0.38$ ), while the Link layer becomes less entangled with higher layers ( $\approx 0.15\text{--}0.22$ ). This aligns with the goal of strengthening consensus where it is most task-relevant, while preserving space for layer-specific cues. Task relevance follows a similar trend. Fig. 5b visualizes the representational transformation achieved by PACC. As indicated by the dashed arrows, all layers undergo a dramatic shift from the high-redundancy, low-relevance region (bottom-right) toward the ideal high-information, low-redundancy zone (top-left). While raw layers are scattered across a wide range of inefficiency (compressing  $11\times\text{--}33\times$ ), PACC unifies them into a highly compact latent space (ratio  $\approx 2\times$ ) with significantly amplified task relevance ( $I(X; Y)$ ), effectively distilling sparse signals from noisy protocols.

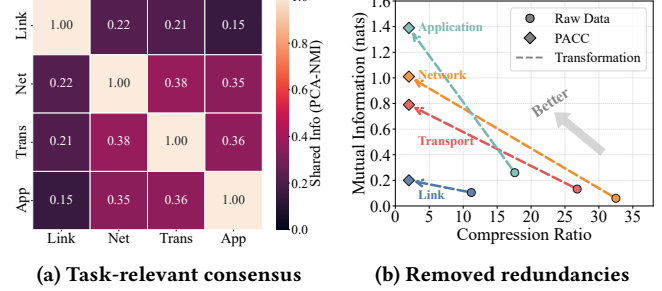


**Figure 5: Layer-wise perspective on NMI and compression of PACC embeddings.** (a) Cross-layer PCA-normalized conditional mutual information  $I(X_i; X_j | Y)$ . (b) Comparison of task relevance  $I(X; Y)$  and redundancy (compression ratio) between raw features and learned representations.

### 5.3 Ablation Study

We benchmark PACC against the *nPrint* baseline (optimized solely by global classification loss) to validate our hierarchical design. As shown in Table 2, sequentially removing objectives reveals their distinct theoretical roles: (i) *w/o Task-Info* suffers the most severe degradation, confirming that maximizing  $I(Z_i; Y)$  is not merely a classification objective but a dual-purpose semantic filter; it purges *task-irrelevant noise* which might be shared but useless while simultaneously excavating the *non-redundant* unique value of each layer, ensuring that both shared and layer-specific evidence contribute to the decision. (ii) *w/o Consensus* validates that the contrastive

**Table 2: Ablation Study of Optimization Objectives (Accuracy).** Note: CS denotes CipherSpectrum.

Variant	CS-1	CS-2	CS-3	CS-4
w/ Classifier (nPrint)	0.6455	0.5590	0.7653	0.6488
w/o Reconstruction	0.7012	0.6388	0.8402	0.7640
w/o Consensus	0.6845	0.6358	0.8438	0.7492
w/o Task-Info	0.6810	0.6364	0.8249	0.7331
<b>PACC</b>	<b>0.7155</b>	<b>0.6602</b>	<b>0.8575</b>	<b>0.7829</b>

alignment is essential for bridging the semantic gap between heterogeneous protocols; without it, the model fails to form a robust shared cross-layer anchor while capturing valuable semantic redundancy that serves as robust evidence for classification. (iii) *w/o Reconstruction* confirms that  $\mathcal{L}_{\text{rec}}$  serves as a foundational regularizer, necessary to compress the *syntactic redundancy* of sparse nPrint inputs, ensuring the faithful preservation of raw information volume and recovering intrinsic directional patterns before semantic processing. The performance drops observed in all ablated variants demonstrate that jointly optimizing these complementary objectives is requisite for achieving the performance upper bound.

#### 5.4 Efficiency and Performance Analysis

To evaluate the trade-off, we compared our method with nPrint and two SOTA pre-training baselines on CipherSpectrum-4, maintaining identical experimental conditions (e.g., batch size, learning rate) (Fig. 6). *Regarding pre-stage overhead*, SOTA methods incur significant costs (e.g., YaTC  $\approx 1.5$ h) under partial dataset evaluation, due to the “pre-train and fine-tune” paradigm requiring learning representations from massive datasets. In contrast, PACC and nPrint avoid this by limiting pre-stage costs strictly to data pre-processing, reducing initial overhead to one-fifth. *In terms of training dynamics*, while pre-trained SOTA models fine-tune quickly due to prior knowledge, PACC surprisingly achieves higher training efficiency (shorter  $T_{\text{train}}$ ) than the simpler nPrint baseline. We attribute this to superior feature consensus modeling, which facilitates faster convergence to the optimal solution compared to the baseline. *Overall*, PACC achieves the highest accuracy of 78.29% with a total time of only 0.57 hours, outperforming SOTA methods in accuracy while maintaining the efficiency.

#### 5.5 Sensitivity Analysis

**5.5.1 Impact of Representation Dimension.** To investigate the influence of the final representation dimension (i.e., the input dimension of the classifier), We evaluated dimensions from 64 to 1024 (Fig. 7). The model exhibits robustness even at lower dimensions, as the reconstruction loss compels the encoder to preserve intrinsic semantics within compact representations. Conversely, excessive dimensions (e.g., 1024) cause performance decline. We attribute this to the re-introduction of sparsity and redundancy, which increases the risk of overfitting and hinders convergence. Therefore, 256 is selected to balance expressiveness and efficiency.

**5.5.2 Impact of Class-balancing Factor  $\beta$ .** Fig. 8 evaluates the introduced class-balance parameter  $\beta$  on the UNSW 2018 dataset. At the baseline  $\beta = 0$ , high accuracy is deceptive due to bias toward majority classes, as revealed by low macro-averaged scores. Performance

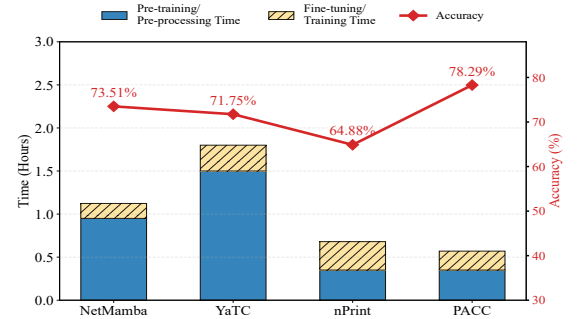


**Figure 6: Comparison of computational efficiency and performance.** The blue bars indicate pre-training time (for SOTA models) or data pre-processing time (for nPrint and PACC). The yellow hatched bars represent the fine-tuning or training time required to reach peak accuracy. The red line traces the highest accuracy achieved by each method.

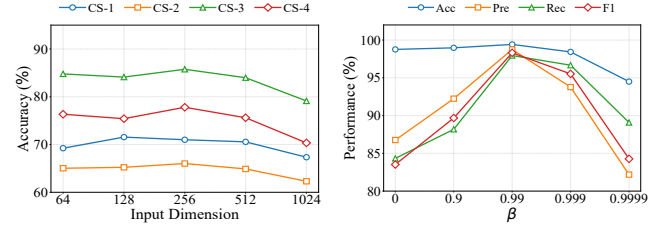


**Figure 7: Impact of the representation dimension.**

**Figure 8: Impact of the class-balancing factor  $\beta$ .**

improves with  $\beta$ , peaking at 0.99. However, pushing  $\beta$  towards 1.0 (e.g., 0.9999) degrades performance; this regime approximates inverse class frequency weights, causing the model to overfit minority outliers and distort decision boundaries. Thus, we fix  $\beta = 0.99$  to achieve a balance between tail supervision and stability.

## 6 Conclusion and Future Work

We introduce PACC, a redundancy-aware cross-layer representation framework that addresses the performance-efficiency bottleneck in encrypted traffic classification. By jointly optimizing layer-wise reconstruction, cross-layer consensus alignment, and task-relevant information, PACC distills compact, discriminative embeddings from noisy raw bitstreams. Extensive experiments on multiple real-world datasets show that our approach outperforms feature-engineered and raw-bit baselines, achieving accuracy comparable to large pre-trained models while reducing training and inference time. A natural next step is to extend the framework to session- and multi-flow settings by modeling temporal dependencies and cross-flow interactions and associated redundancy (e.g., burst structure across flows, host-level aggregation, and graph context). Another important direction is to harden PACC against adversarial and privacy-sensitive environments. For example, the robustness to evasion strategies (e.g., as padding and header manipulation) could be investigated, which could better inform the training objectives that enforce invariances without sacrificing discriminative power.

## References

[1] Andrew Chu, Xi Jiang, Shinan Liu, Arjun Bhagoji, Francesco Bronzino, Paul Schmitt, and Nick Feamster. 2025. NetSSM: Multi-Flow and State-Aware Network Trace Generation using State-Space Models. *arXiv preprint arXiv:2503.22663* (2025).

[2] Yin Cui, Menglin Jia, Tsung-Yi Lin, Yang Song, and Serge Belongie. 2019. Class-Balanced Loss Based on Effective Number of Samples. In *CVPR*.

[3] Google LLC. 2026. HTTPS encryption on the web. <https://transparencyreport.google.com/https/overview?hl=en>. Accessed: 2026-02-01.

[4] Zhaochen Guo, Zhixiang Shen, Xuanting Xie, Liangjian Wen, and Zhao Kang. 2025. Disentangling homophily and heterophily in multimodal graph clustering. In *Proceedings of the 33rd ACM International Conference on Multimedia*. 2044–2053.

[5] Ragini Gupta, Shinan Liu, Ruixiao Zhang, Xinyue Hu, Xiaoyang Wang, Hadjer Benkraouda, Pranav Kommaraju, Phuong Cao, Nick Feamster, and Klara Nahrstedt. 2025. Generative active adaptation for drifting and imbalanced network intrusion detection. *arXiv preprint arXiv:2503.03022* (2025).

[6] Satyandra Guthula, Roman Beltiukov, Navya Battula, Wenbo Guo, and Arpit Gupta. 2023. netFound: Foundation model for network security. *arXiv preprint arXiv:2310.17025* (2023).

[7] Jordan Holland, Paul Schmitt, Nick Feamster, and Prateek Mittal. 2021. New directions in automated traffic analysis. In *Proceedings of the 2021 ACM SIGSAC conference on computer and communications security*. 3366–3383.

[8] Ting-Li Huo, Yan Luo, Peilong Li, and Tong Zhang. 2022. Flow-based encrypted network traffic classification with graph neural networks. *IEEE Transactions on Network and Service Management* 20, 2 (2022), 1224–1237.

[9] Xi Jiang, Shinan Liu, Aaron Gember-Jacobson, Arjun Nitin Bhagoji, Paul Schmitt, Francesco Bronzino, and Nick Feamster. 2024. Netdiffusion: Network data augmentation through protocol-constrained traffic generation. *Proceedings of the ACM on Measurement and Analysis of Computing Systems* 8, 1 (2024), 1–32.

[10] Xi Jiang, Shinan Liu, Saloua Naama, Francesco Bronzino, Paul Schmitt, and Nick Feamster. 2025. JITI: Dynamic Model Serving for Just-in-Time Traffic Inference. *Proceedings of the ACM on Networking* 3, CoNEXT4 (2025), 1–24.

[11] Umakant Kulkarni, Khaled Diab, Lianjie Cao, Faraz Ahmed, Shivang Aggarwal, Puneet Sharma, and Sonia Fahmy. 2025. Maestro: QoE-Aware Dynamic Resource Allocation in Wi-Fi Networks. *Proc. ACM Netw.* 3, CoNEXT1, Article 4 (March 2025), 24 pages. doi:10.1145/3709371

[12] Ronghua Li, Shinan Liu, Haibo Hu, Qingqing Ye, and Nick Feamster. 2025. WiFinger: Fingerprinting Noisy IoT Event Traffic Using Packet-level Sequence Matching. *arXiv preprint arXiv:2508.03151* (2025).

[13] Paul Pu Liang, Zihao Deng, Martin Ma, James Zou, Louis-Philippe Morency, and Ruslan Salakhutdinov. 2023. Factorized Contrastive Learning: Going Beyond Multi-view Redundancy. In *Advances in Neural Information Processing Systems*.

[14] Xinjie Lin, Gang Xiong, Gaopeng Gou, Zhen Li, Junzheng Shi, and Jing Yu. 2022. Et-ber: A contextualized datagram representation with pre-training transformers for encrypted traffic classification. In *Proceedings of the ACM Web Conference 2022*. 633–642.

[15] Chang Liu, Longtao He, Gang Xiong, Zigang Cao, and Zhen Li. 2019. FS-Net: A Flow Sequence Network For Encrypted Traffic Classification. In *IEEE INFOCOM 2019 - IEEE Conference on Computer Communications*. 1171–1179. doi:10.1109/ INFOCOM.2019.8737507

[16] Lingbo Liu, Jiajie Zhen, Guanbin Li, Geng Zhan, Zhaocheng He, Bowen Du, and Liang Lin. 2021. Dynamic Spatial-Temporal Representation Learning for Traffic Flow Prediction. *IEEE Transactions on Intelligent Transportation Systems* 22, 11 (2021), 7169–7183. doi:10.1109/TITS.2020.3002718

[17] Shinan Liu, Francesco Bronzino, Paul Schmitt, Arjun Nitin Bhagoji, Nick Feamster, Hector Garcia Crespo, Timothy Coyle, and Brian Ward. 2023. Leaf: Navigating concept drift in cellular networks. *Proceedings of the ACM on Networking* 1, CoNEXT2 (2023), 1–24.

[18] Shinan Liu, Tarun Mangla, Ted Shaowang, Jinjin Zhao, John Paparrizos, Sanjay Krishnan, and Nick Feamster. 2023. Amir: Active multimodal interaction recognition from video and network traffic in connected environments. *Proceedings of the ACM on Interactive, Mobile, Wearable and Ubiquitous Technologies* 7, 1 (2023), 1–26.

[19] Shinan Liu, Ted Shaowang, Gerry Wan, Jeewon Chae, Jonatas Marques, Sanjay Krishnan, and Nick Feamster. 2024. Serveflow: A fast-slow model architecture for network traffic analysis. *arXiv preprint arXiv:2402.03694* (2024).

[20] Mohammad Lotfollahi, Mahdi Jafari Siavoshani, Ramin Shirali Hosseini Zade, and Mohammdsadegh Saberian. 2020. Deep packet: A novel approach for encrypted traffic classification using deep learning. *Soft Computing* 24, 3 (2020), 1999–2012.

[21] Tarun Mangla, Emir Halepovic, Mostafa Ammar, and Ellen Zegura. 2018. emimic: Estimating http-based video qoe metrics from encrypted network traffic. In *2018 Network Traffic Measurement and Analysis Conference (TMA)*. IEEE, 1–8.

[22] Xuying Meng, Yequan Wang, Runxin Ma, Haitong Luo, Xiang Li, and Yujun Zhang. 2022. Packet representation learning for traffic classification. In *Proceedings of the 28th ACM SIGKDD Conference on Knowledge Discovery and Data Mining*. 3546–3554.

[23] Yisroel Mirsky, Tomer Doitshman, Yuval Elovici, and Asaf Shabtai. 2018. Kit-sune: An Ensemble of Autoencoders for Online Network Intrusion Detection. *arXiv:1802.09089* [cs.CR]. <https://arxiv.org/abs/1802.09089>

[24] Basil Mustafa, Carlos Riquelme, Joan Puigcerver, Rodolphe Jenatton, and Neil Houlsby. 2022. Multimodal contrastive learning with limoe: the language-image mixture of experts. *Advances in Neural Information Processing Systems* 35 (2022), 9564–9576.

[25] Euclides Carlos Pinto Neto, Sajjad Dadkhah, Raphael Ferreira, Alireza Zohourian, Rongxing Lu, and Ali A. Ghorbani. 2023. CICIoT2023: A Real-Time Dataset and Benchmark for Large-Scale Attacks in IoT Environment. *Sensors* 23, 13 (2023). doi:10.3390/s23135941

[26] Aaron van den Oord, Yazhe Li, and Oriol Vinyals. 2018. Representation learning with contrastive predictive coding. *arXiv preprint arXiv:1807.03748* (2018).

[27] Lingfeng Peng, Xiaohui Xie, Sijiang Huang, Ziyi Wang, and Yong Cui. 2024. Ptu: Pre-Trained Model for Network Traffic Understanding. In *32nd IEEE International Conference on Network Protocols, ICNP 2024, Charleroi, Belgium, October 28–31, 2024*. IEEE, 1–12. doi:10.1109/ICNP61940.2024.10858503

[28] Alec Radford, Jong Wook Kim, Chris Hallacy, Aditya Ramesh, Gabriel Goh, Sandhini Agarwal, Girish Sastry, Amanda Askell, Pamela Mishkin, Jack Clark, et al. 2021. Learning transferable visual models from natural language supervision. In *International conference on machine learning*. PMLR, 8748–8763.

[29] Benjamin J Radford, Leonardo M Apolonio, Antonio J Trias, and Jim A Simpson. 2018. Network traffic anomaly detection using recurrent neural networks. *arXiv preprint arXiv:1803.10769* (2018).

[30] Eric Rescorla. 2018. *Transport Layer Security (TLS) Protocol Version 1.3*. RFC 8446. Internet Engineering Task Force (IETF). <https://datatracker.ietf.org/doc/html/rfc8446> IETF Standards Track Document.

[31] Peter J Rousseeuw. 1987. Silhouettes: a graphical aid to the interpretation and validation of cluster analysis. *Journal of computational and applied mathematics* 20 (1987), 53–65.

[32] Ted Shaowang, Shinan Liu, Jonatas Marques, Nick Feamster, and Sanjay Krishnan. 2025. Algorithmic Data Minimization for Machine Learning over Internet-of-Things Data Streams. *arXiv preprint arXiv:2503.05675* (2025).

[33] Toshiki Shibahara, Takeshi Yagi, Mitsuaki Akiyama, Daiki Chiba, and Takeshi Yada. 2016. Efficient dynamic malware analysis based on network behavior using deep learning. In *2016 IEEE Global Communications Conference (GLOBECOM)*. IEEE, 1–7.

[34] Arunam Sivanathan, Hassan Habibi Gharakheili, Franco Loi, Adam Radford, Chamith Wijenayake, Arun Vishwanath, and Vijay Sivaraman. 2018. Classifying IoT Devices in Smart Environments Using Network Traffic Characteristics. *IEEE Transactions on Mobile Computing (TMC)* 18, 8 (Aug 2018), 1745–1759. doi:10.1109/TMC.2018.2866249

[35] Vincent F Taylor, Riccardo Spolaor, Mauro Conti, and Ivan Martinovic. 2017. Robust smartphone app identification via encrypted network traffic analysis. *IEEE Transactions on Information Forensics and Security* 13, 1 (2017), 63–78.

[36] Yonglong Tian, Dilip Krishnan, and Phillip Isola. 2020. Contrastive multiview coding. In *European conference on computer vision*. Springer, 776–794.

[37] Van Tran, Shinan Liu, Tian Li, and Nick Feamster. 2025. Quantifying the Privacy Implications of High-Fidelity Synthetic Network Traffic. *arXiv preprint arXiv:2511.20497* (2025).

[38] Yao-Hung Hubert Tsai, Shaojie Bai, Paul Pu Liang, J Zico Kolter, Louis-Philippe Morency, and Ruslan Salakhutdinov. 2019. Multimodal transformer for unaligned multimodal language sequences. In *Proceedings of the conference. Association for computational linguistics. Meeting*. Vol. 2019. 6558.

[39] Thijs Van Ede, Riccardo Bortolameotti, Andrea Continella, Jingjing Ren, Daniel J Dubois, Martina Lindorfer, David Choffnes, Maarten Van Steen, and Andreas Peter. 2020. Flowprint: Semi-supervised mobile-app fingerprinting on encrypted network traffic. In *Network and distributed system security symposium (NDSS)*, Vol. 27.

[40] Gerry Wan, Shinan Liu, Francesco Bronzino, Nick Feamster, and Zakir Durumeric. 2025. CATO: End-to-End Optimization of {ML-Based} Traffic Analysis Pipelines. In *22nd USENIX Symposium on Networked Systems Design and Implementation (NSDI 25)*. 1523–1540.

[41] Tongze Wang, Xiaohui Xie, Wenduo Wang, Chuyi Wang, Youjian Zhao, and Yong Cui. 2024. Netmamba: Efficient network traffic classification via pre-training unidirectional mamba. In *2024 IEEE 32nd International Conference on Network Protocols (ICNP)*. IEEE, 1–11.

[42] Wei Wang, Ming Zhu, Jinlin Wang, Xuewen Zeng, and Zhongzhen Yang. 2017. End-to-end encrypted traffic classification with one-dimensional convolutional neural networks. In *2017 IEEE International Conference on Intelligence and Security Informatics, ISI 2017, Beijing, China, July 22–24, 2017*. IEEE, 43–48. doi:10.1109/ISI.2017.8004872

[43] Wei Wang, Ming Zhu, Xuewen Zeng, Xiaozhou Ye, and Yiqiang Sheng. 2017. Malware traffic classification using convolutional neural network for representation learning. In *2017 International conference on information networking (ICOIN)*. IEEE, 712–717.

[44] Nimesha Wickramasinghe, Arash Shaghaghi, Gene Tsudik, and Sanjay Jha. 2025. SoK: Decoding the Enigma of Encrypted Network Traffic Classifiers. In *2025 IEEE*

*Symposium on Security and Privacy (SP)*. IEEE Computer Society, Los Alamitos, CA, USA, 1825–1843. doi:10.1109/SP61157.2025.00165

[45] Xi Xiao, Wentao Xiao, Rui Li, Xiapu Luo, Haitao Zheng, and Shutao Xia. 2022. EBSNN: Extended Byte Segment Neural Network for Network Traffic Classification. *IEEE Transactions on Dependable and Secure Computing* 19, 5 (2022), 3521–3538. doi:10.1109/TDSC.2021.3101311

[46] Weisi Yang, Shinan Liu, Feng Xiao, Nick Feamster, and Stephen Xia. 2025. Towards Scalable Defenses against Intimate Partner Infiltrations. *arXiv preprint arXiv:2502.03682* (2025).

[47] Yucheng Yin, Zinan Lin, Minhao Jin, Giulia Fanti, and Vyas Sekar. 2022. Practical gan-based synthetic ip header trace generation using netshare. In *Proceedings of the ACM SIGCOMM 2022 Conference*. 458–472.

[48] Xin Yuan, Zhe Lin, Jason Kuen, Jianming Zhang, Yilin Wang, Michael Maire, Ajinkya Kale, and Baldo Faieta. 2021. Multimodal contrastive training for visual representation learning. In *Proceedings of the IEEE/CVF conference on computer vision and pattern recognition*. 6995–7004.

[49] Amir Zadeh, Minghai Chen, Soujanya Poria, Erik Cambria, and Louis-Philippe Morency. 2017. Tensor fusion network for multimodal sentiment analysis. *arXiv preprint arXiv:1707.07250* (2017).

[50] Haozhen Zhang, Le Yu, Xi Xiao, Qing Li, Francesco Mercaldo, Xiapu Luo, and Qixu Liu. 2023. TFE-GNN: A Temporal Fusion Encoder Using Graph Neural Networks for Fine-grained Encrypted Traffic Classification. In *Proceedings of the ACM Web Conference 2023 (Austin, TX, USA) (WWW ’23)*. Association for Computing Machinery, New York, NY, USA, 2066–2075. doi:10.1145/3543507.3583227

[51] Ruijie Zhao, Mingwei Zhan, Xianwen Deng, Yanhao Wang, Yijun Wang, Guan Gui, and Zhi Xue. 2023. Yet another traffic classifier: A masked autoencoder based traffic transformer with multi-level flow representation. In *Proceedings of the AAAI Conference on Artificial Intelligence*, Vol. 37. 5420–5427.

[52] Guangmeng Zhou, Xiongwen Guo, Zhuotao Liu, Tong Li, Qi Li, and Ke Xu. 2025. Trafficformer: an efficient pre-trained model for traffic data. In *2025 IEEE Symposium on Security and Privacy (SP)*. IEEE, 1844–1860.

[53] Hang Zhu, Varun Gupta, Satyajeet Singh Ahuja, Yuandong Tian, Ying Zhang, and Xin Jin. 2021. Network planning with deep reinforcement learning. In *Proceedings of the 2021 ACM SIGCOMM 2021 Conference*. 258–271.

## A Theoretical Analysis

### A.1 Proof of Proposition 4.1

**Proposition 4.1.** *Minimizing the reconstruction loss  $\mathcal{L}_{rec}^i$  is equivalent to maximizing the variational lower bound of the mutual information  $I(X_i; Z_i)$ , thereby encouraging the latent representation  $Z_i$  to retain faithful, layer-specific information.*

**Lemma A.1** (Variational Lower Bound). *For any two random variables  $U, V$  such that the marginal entropy  $H(U)$  is finite, the mutual information  $I(U; V)$  is bounded from below by the expected log-likelihood of a variational approximation  $q_\theta(U | V)$  to the true posterior  $p(U | V)$ :*

$$I(U; V) \geq H(U) + \mathbb{E}_{p(u, v)} [\log q_\theta(U | V)]. \quad (12)$$

PROOF. The mutual information is defined as  $I(U; V) = H(U) - H(U | V)$ . Utilizing the non-negativity of the Kullback-Leibler divergence  $D_{KL}(p(u | v) \| q_\theta(u | v)) \geq 0$ , we have:

$$-H(U | V) = \mathbb{E}_{p(u, v)} [\log p(u | v)] \geq \mathbb{E}_{p(u, v)} [\log q_\theta(u | v)]. \quad (13)$$

Substituting this inequality back into the definition of mutual information yields the lower bound.  $\square$

**Lemma A.2** (vMF Likelihood and Cosine Equivalence). *Let  $x, \mu \in \mathbb{S}^{d-1}$  be unit vectors such that  $\|x\| = \|\mu\| = 1$ . If a random variable  $x$  follows a von Mises-Fisher distribution with mean direction  $\mu$  and concentration  $\kappa > 0$ , i.e.,  $x \sim vMF(\mu, \kappa)$ , then maximizing the log-likelihood of  $x$  given  $\mu$  is equivalent to minimizing the cosine distance:*

$$\operatorname{argmax}_{\mu} \log P_{vMF}(x | \mu, \kappa) \iff \operatorname{argmin}_{\mu} (1 - \mu^\top x). \quad (14)$$

PROOF. The vMF probability density function is  $f(x; \mu, \kappa) = C_d(\kappa) \exp(\kappa \mu^\top x)$ . The log-likelihood is  $\mathcal{L} = \log C_d(\kappa) + \kappa \mu^\top x$ . Since  $\kappa > 0$  and  $C_d(\kappa)$  are constants with respect to  $\mu$ , maximizing  $\mathcal{L}$  corresponds to maximizing  $\mu^\top x$ . For unit vectors,  $\mu^\top x = \cos \theta$ ; thus, maximizing similarity is equivalent to minimizing the distance  $1 - \mu^\top x$ .  $\square$

PROOF. We now proceed to the main proof. Our objective is to maximize the mutual information  $I(X_i; Z_i)$  between the raw features  $X_i \in \mathbb{R}^{d_f}$  and the latent representation  $Z_i$ . Since the nPrint features are discrete and finite, the marginal entropy  $H(X_i)$  is finite. Applying Lemma A.1 with  $U = X_i$  and  $V = Z_i$ , maximizing  $I(X_i; Z_i)$  is equivalent to maximizing the expected log-likelihood of the variational decoder  $q_\phi(X_i | Z_i)$ :

$$\max_{\phi} \mathcal{J} = \max_{\phi} \mathbb{E}_{p(x, z)} [\log q_\phi(X_i | Z_i)]. \quad (15)$$

To capture the directional semantics of the traffic features, we explicitly account for the geometric nature of nPrint embeddings. Specifically, since the semantic identity of these binary vectors is encoded strictly in the *spatial pattern* of active bits (i.e., the vector orientation) rather than their magnitude, we define the normalized input as  $x = X_i / \|X_i\|$  and the mean direction parameter as  $\mu = \hat{X}_i / \|\hat{X}_i\|$ , where  $\hat{X}_i = g_\phi(Z_i)$  is the output of the up-projecting decoder. Crucially, the normalization operations ensure that both  $x$  and  $\mu$  satisfy the unit norm constraint ( $\|\mu\| = 1$ ) required by Lemma A.2.

By invoking Lemma A.2, the maximization of the expected vMF log-likelihood transforms directly into the minimization of the

expected cosine distance. Consequently, we can rewrite the optimization objective by substituting the normalized vectors back into the distance formulation:

$$\max_{\phi} \mathcal{J} \iff \min_{\phi} \mathbb{E} [1 - \mu^T x] = \min_{\phi} \mathbb{E} \left[ 1 - \frac{X_i^T \hat{X}_i}{\|X_i\| \|\hat{X}_i\|} \right]. \quad (16)$$

This final expression corresponds exactly to the formulation of our reconstruction loss  $\mathcal{L}_{\text{rec}}$  in Eq. (2), completing the proof.  $\square$

## A.2 Proof of Theorem 4.1

**Theorem 4.1.** *Equivalence of Shared and Holistic Mutual Information.* Maximizing the MI between the holistic representations  $Z_i$  and  $Z_j$  is equivalent to maximizing the MI between their shared components  $Z_i^s$  and  $Z_j^s$ . Under the independence assumptions in Definition 4.1, the identity  $I(Z_i; Z_j) = I(Z_i^s; Z_j^s)$  holds.

**PROOF.** Let  $Z_i = (Z_i^s, Z_i^u)$  and  $Z_j = (Z_j^s, Z_j^u)$ . By the chain rule for mutual information, we expand  $I(Z_i; Z_j)$  as:

$$\begin{aligned} I(Z_i; Z_j) &= I((Z_i^s, Z_i^u); Z_j) \\ &= I(Z_i^s; Z_j) + I(Z_i^u; Z_j | Z_i^s). \end{aligned} \quad (17)$$

By Definition 4.1 (Conditional Latent Decomposition Assumption), the private component is conditionally independent of other layer representations given the shared component:

$$Z_i^u \perp Z_j | Z_i^s \Rightarrow I(Z_i^u; Z_j | Z_i^s) = 0.$$

Substituting this into (17) yields:

$$I(Z_i; Z_j) = I(Z_i^s; Z_j). \quad (18)$$

Since the symmetric assumption also holds for  $Z_j$ , i.e.,  $Z_j^u \perp Z_i | Z_j^s$ , we can further apply the chain rule:

$$\begin{aligned} I(Z_i^s; Z_j) &= I(Z_i^s; (Z_j^s, Z_j^u)) \\ &= I(Z_i^s; Z_j^s) + I(Z_i^s; Z_j^u | Z_j^s). \end{aligned} \quad (19)$$

Using the symmetric conditional independence:

$$Z_j^u \perp Z_i | Z_j^s \Rightarrow Z_j^u \perp Z_i^s | Z_j^s \Rightarrow I(Z_i^s; Z_j^u | Z_j^s) = 0,$$

we finally obtain:

$$I(Z_i; Z_j) = I(Z_i^s; Z_j^s). \quad (20)$$

$\square$

## A.3 Proof of Proposition 4.2

**Proposition 4.2.** *Optimization and Decomposition of Task-Relevant Information.* Maximizing the total task-relevant information  $I(Z_i; Y)$  is mathematically equivalent to minimizing the standard cross-entropy loss  $\mathcal{L}_{\text{ce}}$  via a variational lower bound. Furthermore, this optimization implicitly maximizes two complementary information components:

(1) *Inter-Layer decomposition: The sum of layer-specific evidence and cross-layer consensus:*

$$I(Z_i; Y) = I(Z_i; Y | Z_{-i}) + I(Z_i; Z_{-i}; Y). \quad (5)$$

(2) *Intra-Layer decomposition: The sum of private feature utility and shared feature utility conditioned on private features:*

$$I(Z_i; Y) = I(Z_i^u; Y) + I(Z_i^s; Y | Z_i^u). \quad (6)$$

**PROOF.** We first address the tractability. Direct estimation of  $I(Z_i; Y)$  is intractable. By introducing a variational distribution  $q_{\theta}(Y | Z_i)$  to approximate the true posterior  $p(Y | Z_i)$  (see Lemma A.1), and utilizing the entropy decomposition  $I(Z_i; Y) = H(Y) - H(Y | Z_i)$ , we derive the lower bound:

$$\begin{aligned} I(Z_i; Y) &= H(Y) - H(Y | Z_i) \\ &\geq H(Y) + \mathbb{E}_{p(Z_i, Y)} [\log q_{\theta}(Y | Z_i)]. \end{aligned} \quad (21)$$

Since  $H(Y)$  is constant, maximizing the lower bound is equivalent to minimizing the negative log-likelihood, yielding the cross-entropy loss  $\mathcal{L}_{\text{ce}}$ .

Next, we derive the inter-layer decomposition (Eq. 5). Using the definition of conditional mutual information  $I(Z_i; Y | Z_{-i}) = H(Y | Z_{-i}) - H(Y | Z_i, Z_{-i})$ , we expand the interaction term:

$$\begin{aligned} I(Z_i; Y) - I(Z_i; Y | Z_{-i}) &= H(Y) - H(Y | Z_i) - [H(Y | Z_{-i}) - H(Y | Z_i, Z_{-i})] \\ &= I(Z_i; Z_{-i}; Y). \end{aligned} \quad (22)$$

Finally, for the intra-layer decomposition (Eq. 6), recall that  $Z_i = (Z_i^s, Z_i^u)$ . Applying the chain rule of mutual information the objective decomposes as:

$$\begin{aligned} I(Z_i; Y) &= I(Z_i^s, Z_i^u; Y) \\ &= I(Z_i^u; Y) + I(Z_i^s; Y | Z_i^u). \end{aligned} \quad (23)$$

$\square$

## B Experimental Details

**Baselines.** In our comparative analysis, we consider various state-of-the-art methods for comprehensive evaluation. The first category comprises flow statistics approaches reliant on manual feature engineering, such as AppScanner [35] and FlowPrint [39]. The second category involves raw-bit/byte encoding methods exemplified by TFE-GNN[?] and nPrint [7]. For the reproduction of nPrint, we adopt its specific feature encoding scheme and subsequently feed the generated representations into a classifier for performance evaluation. The third category encompasses pre-training paradigms, including YaTC [51] and Netmamba [41]. For these models, we leverage their open-source pre-trained weights and perform fine-tuning on our specific downstream tasks.

**Metrics.** The performance of our model is quantified using a comprehensive suite of four evaluation metrics: Accuracy (ACC), and the macro-averaged Precision (PRE), Recall (REC), and F1-score (F1).

**Implementation Details.** *Data Preparation.* Each raw PCAP file is partitioned into individual bidirectional flows. To standardize the input representation, we segment each flow into a fixed length based on packet granularity, applying truncation or zero-padding where necessary. We apply a unified splitting strategy across all experiments: an 8:1:1 ratio for large-scale datasets, and a 9:1 training-test split for small-scale categories like CipherSpectrum subsets. To ensure model robustness and avoid "shortcuts" identified in recent literature [44], we strictly adhere to their artifact masking protocols across the L2, L3, L4, and L7 layers or even directly remove such shortcuts, to prevent the model from learning spurious correlations or overfitting to temporal session states. This

Table 3: Overview of Datasets and Statistics.

Dataset	Classes	Raw Size	Flow-level Captures	Application
CipherSpectrum-1 [44]	11	194 MB	4400	Encrypted Application Classification
CipherSpectrum-2 [44]	10	340 MB	4000	
CipherSpectrum-3 [44]	10	645 MB	4000	
CipherSpectrum-4 [44]	10	285 MB	4000	
UNSW 2018 [34]	16	882 MB	51442	IoT Device Classification
CICIoT 2023 [25]	2	1.61 MB	6076	Attack Traffic Classification

Table 4: Comparison of Network Traffic Classification Methods: Design Choices &amp; Explicit Layer Focus. H/P Distinction? denotes whether the method independently attends to and distinguishes between Header (H) and Payload (P). Explicit Layer Focus indicates the specific network layers providing utilizable representations. Symbols: ✓ = Yes/Distinguished; ✗ = No/Unified; • = Layer Utilized; ○ = Not Utilized.

Category	Method	Design Choice	Explicit Layer Focus			
		H/P Distinction?	Link (L2)	Net (L3)	Trans (L4)	App (L7)
Flow Statistics	AppScanner	✗ (No Content)	○	•	•	○
	FlowPrint	✓ (Explicit Feat.)	○	•	•	•
	FS-Net	✗ (Raw Sequence)	○	•	•	•
Raw Packets	TFE-GNN	✓ (Dual Embed.)	○	•	•	•
	nPrint	✓ (Bit-by-Bit)	•	•	•	•
Pretrained Embedding	PERT	✗ (Payload Only)	○	○	○	•
	ET-BERT	✗ (Mixed Feat.)	○	○	○	•
	YaTC	✓ (MFR Matrix)	○	○	○	•
	NetMamba	✓ (Stride Sequence)	○	○	○	•
Proposed	PACC	✓ (Explicit Fusion)	•	•	•	•

rigorous preprocessing forces the classifier to learn intrinsic, generalizable traffic patterns rather than memorizing specific network configurations or session fingerprints.

*Feature Engineering.* Building upon the preprocessed flows described above, for baseline replication, we utilize raw datagram bytes, while our proposed framework employs nPrint for standardized bit-level flow encoding. We primarily focus on metadata from the Link (L2), Network (L3), and Transport (L4) layers alongside Encrypted Payloads (L7). Notably, for encrypted application classification, we rely exclusively on L3 and L4 headers, as empirical evidence suggests that modern encryption renders intrinsic payload patterns unlearnable beyond their length [44].

*Model Architecture.* To eliminate dimensional redundancy and distill compact latent representations, the architecture implements

a progressive dimensionality reduction strategy. Specifically, the input feature dimension is mapped through consecutive layers to progressively reduced sizes (e.g., 512, 256, and 128 units). This stepwise compression forces the network to filter out non-discriminative features and condense sparse bit-level information. To prevent overfitting during this reduction, a dropout rate of 0.5 is applied across all hidden layers.

*Training Configuration.* We employ the Adam optimizer with an initial learning rate set to  $1.0 \times 10^{-3}$  or  $2.0 \times 10^{-3}$ . To address class imbalance, a class-balanced global classification loss with  $\beta = 0.99$  is introduced to re-weight samples based on their effective volume. All experiments were conducted on a high-performance server equipped with an NVIDIA Tesla V100-32GB GPU and an Intel(R) Xeon(R) Gold 6130 CPU @ 2.10GHz to ensure consistent computational benchmarks.